Strong-coupling perturbative study of the disordered Hubbard model on the honeycomb lattice

Alireza Habibi,[1,2] Elaheh Adibi,[1] and S. A. Jafari[1,3,*]

[1]*Department of Physics, Sharif University of Technology, Tehran 11155-9161, Iran*

[2]*School of Physics, Institute for Research in Fundamental Sciences (IPM), Tehran 19395-5531, Iran*

[3]*Center of Excellence for Complex Systems and Condensed Matter (CSCM), Sharif University of Technology, Tehran 14588-89694, Iran*

(Received 1 July 2018; published 3 December 2018)

We study the Anderson disordered Hubbard model on the honeycomb lattice. The Hubbard term is handled with strong-coupling perturbation theory which encodes the information about Mott transition physics into a rich dynamical local self-energy. The local nature of the self-energy allows us to combine it with kernel polynomial and transfer matrix methods which consequently enables us to study lattices with millions of sites. The transfer matrix method, which in the ribbon geometry is essentially free from finite-size errors, can be employed to perform finite-size scaling on the width of the ribbon. This enables us to rule out the possibility of metallic phase between the Mott and Anderson insulating phases which has been claimed in the literature. Therefore, we find a direct transition between Anderson and Mott insulators when the disorder strength W is comparable to the Hubbard interaction U. For a fixed disorder strength W, we obtain an interaction-dependent nonmonotonic behavior of the localization length which reflects the interaction-induced enhancement of the localization length for weak and intermediate interaction strengths. Eventually, at strong interactions U, the Mott localization takes over, and the localization length becomes comparable to the lattice scale. This phenomenon is reminiscent of the holographic determination of the Mott state where the system at infrared recognizes its ultraviolet lattice scale.

DOI: 10.1103/PhysRevB.98.245105

I. INTRODUCTION

The physical properties of solids are strongly influenced by the interaction between electrons and the presence of disorder. Localization is the most important theme in both purely disordered systems and purely correlated systems. The localization in the above two cases occurs for two completely different reasons. In correlated systems, strong Coulomb interaction strength at half-filling due to the high cost of double occupancy leads to a state with gapped charge excitations which is known as Mott insulator [1]. On the other hand, in the presence of disorder due to coherent backscattering, the eigenstates of the noninteracting system can be localized and decay exponentially with distance which defines the Anderson insulating state [2].

On honeycomb lattice, the semimetal to Mott insulator transition driven by only electron-electron interaction has been extensively studied by various methods such as quantum Monte Carlo (QMC) simulations [3,4], renormalization group methods [5,6], cluster dynamical mean field theory (cDMFT) [7–9], strong-coupling perturbation approach [10], and so on. For disordered and noninteracting electrons on the honeycomb lattice, recent studies have shown that strong long-range disorder [11,12] and short-range disorder [13–16] cause intervalley scattering which leads to Anderson localization. On the other hand, honeycomb lattice as a two-dimensional lattice is a good candidate to consider the scaling theory of localization [17]. This theory predicts that all states of the one- and two-dimensional systems are localized at zero temperature for any finite disorder strength in the absence of electron-electron interaction and magnetic field. Schreiber and Ottomeier [18] and Fan *et al.* [19] by using the transfer matrix method and the real-space Kubo-Greenwood formula, respectively, and Lee *et al.* [20] by means of self-consistent Born approximation showed that in the presence of short-range disorder in graphene, all states are localized and obey the scaling theory of localization. On the other hand, the results of Refs. [21,22] found a metal-insulator transition for uncorrelated and short-range disorder in graphene.

While the individual effects of interaction and disorder are widely examined on the honeycomb lattice, the interplay of interaction and disorder on the honeycomb lattice is a less understood and nontrivial problem. On the other hand, in real materials, both interaction and disorder are present. So, in this paper, we set out to investigate the combined effects of the interaction and disorder on the metal-insulator transition by focusing on the honeycomb lattice.

Despite the extensive research throughout the decades on the competition of interaction and disorder in different lattices, no conclusive theory has been established yet. The challenging problem is the existence of an interaction-induced metallic phase in the two-dimensional materials which has been discussed by many authors. The metallic ground state found in finite-size systems in two dimensions is reported in Refs. [23–26]. It was suggested that the numerically obtained metallic phase in two-dimensional materials is probably an artifact of finite-size effects [27]. The typical numerical methods such as QMC [28,29], exact diagonalization [30], cDMFT [7,31], variational cluster approximation [32,33], that are routinely used to handle the interaction part, suffer from severe size limitations rooted in the exponential growth of the Hilbert

*jafari@physics.sharif.edu

space. Therefore, it would be desirable to employ an analytic procedure to handle the interaction part. To better understand the puzzles on the interplay of interactions and disorder, in this paper we use a method which does not suffer from such severe finite-size effects, that will, in turn, enable us to perform a reliable finite-size scaling. Based on the finite-size scaling, we rule out the possibility of a conducting state between Mott and Anderson insulating states.

Let us briefly sketch the method that we apply to solve the interaction part perturbatively. We employ the so-called strong-coupling perturbation theory [34,35] which can be used to analytically calculate the Green's function of the Hubbard Hamiltonian for infinite lattice sizes. In this method, the intersite hopping t is treated as the perturbation parameter, so that one can carry out the perturbation expansion about the atomic limit in powers of t/U where U is the Hubbard interaction strength. Since the typical values of critical U/t needed for Mott transition are $\sim$3, even a low-order perturbation treatment in $t/U \sim \frac{1}{3}$ can capture the Mott transition. The highly nontrivial information on Mott physics is encoded in the dynamical self-energy that can be analytically computed in this method. This self-energy is local and therefore it can be naturally adapted to disordered situations. This procedure is free from any finite-size artifacts on the Hubbard part. Placing nontrivial (and local) self-energies on a lattice allows us to combine it with onsite Anderson disorder (measured by the width W of the distribution of the onsite energy) that can be numerically solved in a very efficient way. Employing the kernel polynomial method (KPM) allows us to calculate the density of state (DOS) for the disordered interacting system with millions of lattice sites in the real space. In this method, every spectral function is expanded in terms of Chebyshev (or any other complete set of orthonormal) polynomials, where the expansion coefficients are obtained through an efficient recursion relation involving matrix elements of the Hamiltonian in stochastically sampled states [36,37]. The central result obtained from DOS is that in the presence of disorder there is a *direct* transition from Anderson insulator to Mott insulator which takes place at a critical interaction $U_c \approx W$. To obtain further insight into the behavior of the disordered Hubbard model, we utilize the transfer matrix method [38,39] to compute the localization length. The finite-size scaling analysis of the localization length can conclusively determine whether the system is metal or Anderson insulator. The localization length is considered as the relevant scale which determines the transport properties of the system. We do not find any metallic state between the Mott and Anderson insulating states, in agreement with previous numerical results [27,40,41] reported for the Anderson-Hubbard model. For large disorder strength W, by increasing U the localization length increases and after reaching a maximum starts to decrease. The increase in the localization length can be attributed to the screening of disorder by interactions. Our finite-size scaling shows that even the maximal localization length corresponds to Anderson insulating state. Finite-size scaling enables us to rule out a possible metallic state in-between the Anderson and Mott insulating states.

The rest of this paper is organized as follows. We begin by introducing the Anderson-Hubbard model to study the interacting disorder system and then briefly reviewing the strong-coupling approach in Sec. II. Next, in Sec. III, we present our results for the interplay of interaction and disorder. The paper closes with a conclusion in Sec. IV. The paper is accompanied by three appendices. In the first appendix, we present the one-point correlation function of atomic limit of the Hamiltonian. To be self-contained in two other appendices, we describe the KPM and transfer matrix method.

II. MODEL AND METHOD

We study the disordered interacting system within the Anderson-Hubbard model which is given by the following Hamiltonian:

$$\begin{aligned} H &= H_0 + H_1, \\ H_0 &= U \sum_i n_{i\uparrow} n_{i\downarrow} - \mu \sum_{i,\sigma} n_{i\sigma} + \sum_{i,\sigma} \epsilon_i \, n_{i\sigma}, \\ H_1 &= \sum_{ij,\sigma} V_{ij} \, (c^\dagger_{i\sigma} \, c_{j\sigma} + \text{H.c.}), \end{aligned} \tag{1}$$

where H_0 accounts for interaction and disorder energy, and H_1 for kinetic energy. Also, $c^\dagger_{i\sigma}$ and $c_{i\sigma}$ are the fermionic creation and annihilation operators of the particle with spin $\sigma =\uparrow, \downarrow$ on the lattice site i, respectively. The operator $n_{i\sigma} = c^\dagger_{i\sigma} \, c_{i\sigma}$ measures the occupation of site i with an electron of spin σ. V_{ij} is the hopping matrix element between sites i and j. U is the onsite Hubbard repulsion and μ is the chemical potential. The disorder couples to the system through the local term in H_0 which is parametrized with a random scalar potential ϵ_i belonging to a box probability distribution $P(\epsilon_i) = \Theta(W/2 - |\epsilon_i|)/W$, where Θ is the step function. The parameter W is a measure of the disorder strength.

In what follows, we briefly describe the strong-coupling perturbation theory [34]. Considering H_0 and H_1 in Hamiltonian (1) as the unperturbed and perturbed parts, respectively, the partition function at temperature $T = 1/\beta$ is written as

$$\begin{aligned} Z = \int [d\gamma^\star d\gamma] \, \exp\Bigg[- \int_0^\beta d\tau \Bigg\{ \sum_{i\sigma} \gamma^\star_{i\sigma}(\tau) \, \partial_\tau \, \gamma_{i\sigma}(\tau) \\ + \, H_0(\gamma^\star_{i\sigma}(\tau), \gamma_{i\sigma}(\tau)) + \sum_{ij\sigma} \gamma^\star_{i\sigma}(\tau) \, V_{ij} \, \gamma_{j\sigma}(\tau) \Bigg\} \Bigg], \end{aligned} \tag{2}$$

where γ and $\gamma^\star$ denote the Grassmann fields in the imaginary time τ.

In the absence of the Wick's theorem for the unperturbed Hamiltonian, employing the standard perturbation theory is not straightforward. The Wick's theorem is brought to life by applying the following Hubbard-Stratonovich transformation:

$$\begin{aligned} &\int [d\psi^\star d\psi] \exp\Bigg[\int_0^\beta d\tau \sum_{i\sigma} \Bigg\{ \sum_j \psi^\star_{i\sigma}(\tau)(V^{-1})_{ij} \psi_{j\sigma}(\tau) \\ &\quad + \, \psi^\star_{i\sigma}(\tau)\gamma_{i\sigma}(\tau) + \gamma^\star_{i\sigma}(\tau)\psi_{i\sigma}(\tau) \Bigg\} \Bigg] \\ &= \det(V^{-1}) \exp\Bigg[- \int_0^\beta d\tau \sum_{ij\sigma} \gamma^\star_{i\sigma}(\tau) \, V_{ij} \, \gamma_{j\sigma}(\tau) \Bigg], \end{aligned} \tag{3}$$

where $\psi_{i\sigma}(\tau)$ and $\psi^{\star}_{i\sigma}(\tau)$ are the auxiliary Grassmann fields. By means of this transformation, up to a normalization factor, the partition function becomes

$$Z=\int[d\psi^{\star}d\psi]\exp\left[-\left\{S_0[\psi^{\star},\psi]+\sum_{R=1}^{\infty}S^{R}_{\rm int}[\psi^{\star},\psi]\right\}\right]. \quad (4)$$

As can be seen, the new representation of the partition function is in terms of the auxiliary fermions. $S_0[\psi^{\star},\psi]$ is the free auxiliary fermion action determined by the inverse of the hopping matrix of original fermions,

$$S_0[\psi^{\star},\psi]=-\int_0^{\beta}d\tau\sum_{ij\sigma}\psi^{\star}_{i\sigma}(\tau)\,(V^{-1})_{ij}\,\psi_{j\sigma}(\tau), \quad (5)$$

and $S^{R}_{\rm int}[\psi^{\star},\psi]$ includes an infinite number of interaction terms given by

$$\begin{aligned}S^{R}_{\rm int}[\psi^{\star},\psi]=\frac{-1}{(R!)^2}\sum_{i}\sum_{\{\sigma_l\sigma'_l\}}\int_0^{\beta}\prod_{l=1}^{R}d\tau_l d\tau'_l\\ \times\psi^{\star}_{i\sigma_1}(\tau_1)\ldots\psi^{\star}_{i\sigma_R}(\tau_R)\psi_{i\sigma'_R}(\tau'_R)\ldots\psi_{i\sigma'_1}(\tau'_1)\\ \times\langle\gamma_{i\sigma_1}(\tau_1)\ldots\gamma_{i\sigma_R}(\tau_R)\gamma^{\star}_{i\sigma'_R}(\tau'_R)\ldots\gamma^{\star}_{i\sigma'_1}(\tau'_1)\rangle_{0,c},\end{aligned} \quad (6)$$

where $\langle\gamma_{i\sigma_1}(\tau_1)\ldots\gamma_{i\sigma_R}(\tau_R)\gamma^{\star}_{i\sigma'_R}(\tau'_R)\ldots\gamma^{\star}_{i\sigma'_1}(\tau'_1)\rangle_{0,c}$ represents the connected correlation function with respect to the atomic limit Hamiltonian H_0. In the diagrammatic representation, this correlation function denotes a vertex with $2R$ vertices with R incoming (ψ) and R outgoing ($\psi^{\star}$) auxiliary fermions.

In the partition function of the auxiliary fermions (4), the free propagator is given by matrix V. So, we can apply the Wick's theorem to perturbatively incorporate the interaction term (6) and calculate the self-energy of the auxiliary fermion (Γ). Finally, the Green's function of the original fermions is expressed by

$$G=(\Gamma^{-1}-V)^{-1}. \quad (7)$$

For more details on the strong-coupling approach, see Ref. [35].

III. RESULTS

We consider the honeycomb lattice with $V_{ij}=-t$ when i,j are nearest-neighbor sites and zero otherwise. Also, throughout the paper, we set the unit of energy by $t=1$. In graphene this energy scale corresponds to $t\sim 2.8$ eV [42]. We are interested in half-filling which is defined by $\overline{\langle n_{i\sigma}\rangle}=\frac{1}{2}$ where $\langle n_{i\sigma}\rangle$ denotes the mean occupation of each site for a given spin projection and a fixed realization of randomness which is given by the following equation:

$$\langle n_{i\sigma}\rangle=\frac{e^{\beta(U/2-\epsilon_i)}+e^{-2\beta\epsilon_i}}{1+2e^{\beta(U/2-\epsilon_i)}+e^{-2\beta\epsilon_i}}, \quad (8)$$

where ϵ_i are random onsite energies distributed in a box of width W. The bar in $\overline{\langle\ldots\rangle}$ denotes averaging over realizations of disorder. In the absence of ϵ_i term in the Hamiltonian (1), the half-filling is simply realized by setting the chemical potential $\mu=U/2$. In the presence of the disorder term the plot of $\langle n_{i\sigma}\rangle$ as a function of the chemical potential μ at zero temperature consists in three plateaus corresponding to values of 0, 0.5, and 1. For $W<U$, only the portion of plateaus corresponding to 0.5 is realized and therefore $\mu=U/2$ establishes the half-filling. For $W>U$, the occupation $\langle n_{i\sigma}\rangle$ in addition to 0.5 has a chance to pick up 0,1 as well. However, due to the symmetry of Eq. (8) around $\mu=U/2$, the chance of realizing occupation of 0 and 1 is equal. Therefore, again the previously mentioned chemical potential specifies the half-filling. So, in the presence of any disorder, we still use the $\mu=U/2$.

We treat the Mott-Hubbard aspects within the leading order of the strong-coupling perturbation theory which is already capable of capturing the Mott physics. At this order, the dynamical self-energy of the auxiliary fermions is expressed by the one-point connected correlation function (for derivation see Appendix A). So, in this limit the self-energy of the auxiliary fermions at half-filling for each spin is given by

$$\Gamma_{ij}(i\omega)=\left(\frac{1-\langle n_i\rangle}{i\omega-\epsilon_i+U/2}+\frac{\langle n_i\rangle}{i\omega-\epsilon_i-U/2}\right)\delta_{ij}, \quad (9)$$

where $i\omega$ denotes the Matsubara frequency and δ_{ij} is Kronecker delta. Note that according to Hamiltonian (1), in the absence of symmetry breaking, there are no differences between $\langle n_{i\uparrow}\rangle$ and $\langle n_{i\downarrow}\rangle$, so we just use $\langle n_i\rangle$ for mean occupation.

A. Mott gap equation in disordered systems

As discussed in detail in Ref. [10], the strong-coupling perturbation theory enables us to set up a *gap equation* for the Mott state. The DOS of the clean interacting electrons on the honeycomb lattice turns out to be $\rho(\omega)=\rho_0(\Gamma^{-1}(\omega))$ where ρ_0 denotes the DOS of noninteracting electrons. Due to threefold coordination of the honeycomb lattice, ρ_0 is nonzero if and only if the absolute value of its argument does not exceed 3. Therefore, the criterion $|\Gamma^{-1}(\omega+i0^{+})|_{\omega=0}\geqslant 3$ determines the Mott state in clean system. In disordered systems, level repulsion increases the half-bandwidth value from 3. The appropriate generalization of this criterion for disordered systems will be

$$\overline{|\Gamma^{-1}(\omega+i0^{+})|}_{\omega=0}\geqslant B^{0}_{W}, \quad (10)$$

where B^{0}_{W} is the half-bandwidth of the *noninteracting but disordered* system which will now depend on the disorder strength W. This relation simply expresses the disorder-averaged version of the condition that the denominator of Eq. (7) does not pick a pole at $\omega=0$. We stress that the half-bandwidth of the clean and noninteracting system is $B^{0}_{W=0}=3$ [10].

Now, let us see how does Γ^{-1}, which is related to the self-energy of physical electrons, respond to Anderson disorder. As can be seen from Eq. (9), the self-energy Γ of auxiliary fermions parametrically depends on the random onsite energies ϵ_i. Therefore, the random distribution of ϵ_i induces a distribution of Γ which will now be a dynamical distribution as it depends on frequency ω. Figure 1 shows the distribution of $\Gamma^{-1}(\omega)$ at all frequencies for various values of disorder strength W, and a fixed Hubbard interaction $U=6$. Taking advantage of the criterion (10), the important feature

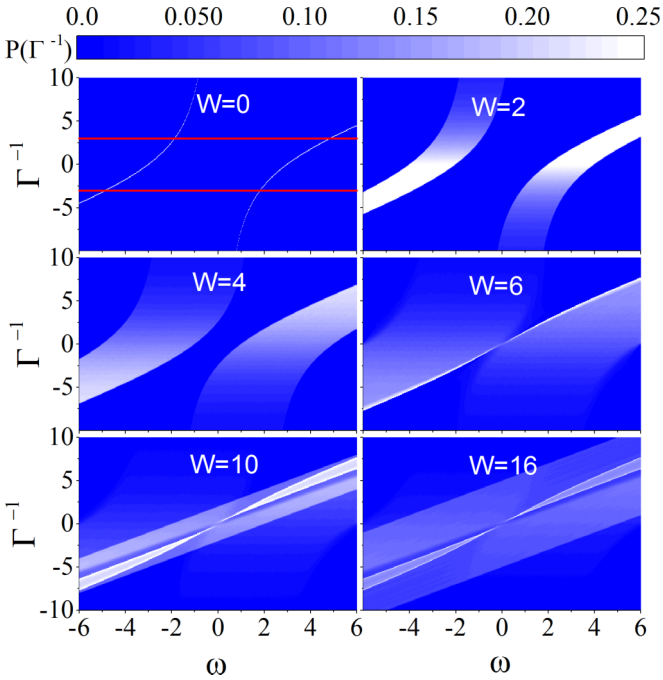

FIG. 1. The distribution of $\Gamma^{-1}(\omega)$ for different disorder strength W at $U = 6$. Red lines in the upper left panel show the critical values $\Gamma^{-1} = \pm 3$ beyond which the Mott state is realized.

obtained from Fig. 1 is that at those frequencies ω where the distribution of Γ^{-1} takes an average value between $-B_W^0$ and B_W^0, the *interacting* DOS at ω will be nonzero. Because of the particle-hole symmetry, the possible Mott-Hubbard gap opens up at $\omega = 0$. So, we focus on zero frequency (i.e., at Fermi energy). As can be seen, in the absence of disorder, $W = 0$ (top left panel in Fig. 1), Γ^{-1} is distributed on a line of zero width. Moreover, at $\omega = 0$, this line distribution already falls outside the range of $(-B_0^0, +B_0^0)$. Therefore, the interacting DOS is gapped for $W = 0$ and $U = 6$ and, consequently, the system is in its Mott insulating phase. By turning on the disorder, the distribution of Γ^{-1} starts to broaden and as demonstrated for $W \geqslant 6$, the distribution of Γ^{-1} will move most of its weight to $\omega = 0$, such that its average at $\omega = 0$ falls within the noninteracting bandwidth specified by B_W^0. Consequently, strong enough disorder closes the Mott gap and the system becomes Anderson insulator. By further increasing the disorder strength, especially the $\omega \approx 0$ portion of – $\Gamma^{-1}(\omega)$ distribution becomes more concentrated in the noninteracting bandwidth B_W^0.

B. Competition between Anderson localization and Mottness

To get a better understanding of what is explained for Fig. 1, we calculate the DOS. In other words, instead of expressing the condition for picking up a nonzero density of states at $\omega = 0$, the relevant trace (Tr) of Eq. (7) is computed. This calculation can be efficiently done with the KPM [36]. However, in the present case, owing to the nonlinear dependence of $\Gamma^{-1}(\omega)$ on ω, we employ a trick which has been explained in Appendix B. We display the disorder-averaged DOS at half-filling and zero temperature in different disorder strengths and $U = 6$ for a lattice with 500×500 sites in

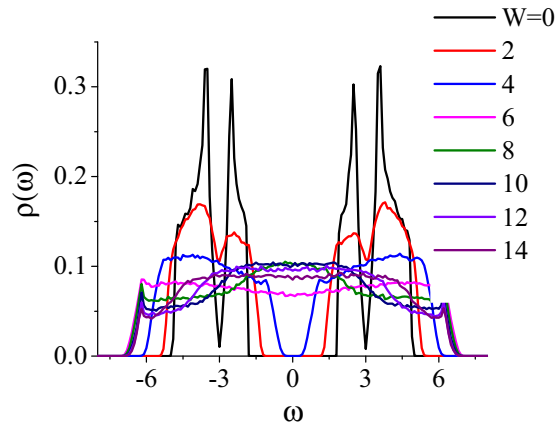

FIG. 2. The evolution of the disorder-averaged DOS as a function of W for fixed $U = 6$ at half-filling and zero temperature.

Fig. 2. Note that the present method, i.e., strong-coupling expansion in t/U, works better for larger U. We have benchmarked the $W = 0$ DOS (black curve) of our KPM algorithm against Ref. [10]. As can be seen in Fig. 2 for $U = 6$ in the absence of disorder, the system has already a Mott gap as expected from Refs. [3,10]. As we pointed out, by turning on the disorder, the DOS gradually broadens and eventually the gap closes at the disorder strength of $W \approx U$. By increasing the disorder, the resulting level repulsion evolves the clear Mott gap into a pseudogap which is subsequently filled, whereby the Mott phase is destroyed. Therefore, we will be dealing with a situation where there are some states present at the Fermi level. Now, the question is whether these states are Anderson localized or extended?

The remarkable feature of DOS is that, since for nonzero disorder the Mott gap is already suppressed, much larger U is required to restore the Mott gap. In other words, the disorder affects the Mott transition by pushing the critical values U_c to larger values, as also reported in Refs. [43,44].

To characterize the nature of the expected phases of the model, let us employ the exact diagonalization to generate a snapshot of the charge density (wave function squared) at Fermi energy which is shown in Fig. 3 for a fixed disorder strength $W = 6$. As illustrated in this figure, the system is Anderson localized for $U = 0.2$ and 0.5, as the charge density consists of disconnected puddles. By increasing the interaction, at $U = 1$ and 2 it appears that the charge puddles percolate and one is tempted to think that these values of U correspond to an intermediate conducting phase. In Refs. [23–25] using the QMC method and in Ref. [26] by self-consistent Hartree-Fock calculations, authors identify the apparent percolating charge density with metallic phase. However, we will shortly show that this metallic phase is an artifact of the small lattices in the above-mentioned works. A careful finite-size scaling based on transfer matrix method will show that the system is still in the Anderson localized phase. Upon further increase of the interaction in Fig. 3, we again have localized state at $U = 4$ and 6. If we continue to increase the Coulomb interaction, the Mott gap appears, and there will be no states at the Fermi level ($\omega = 0$).

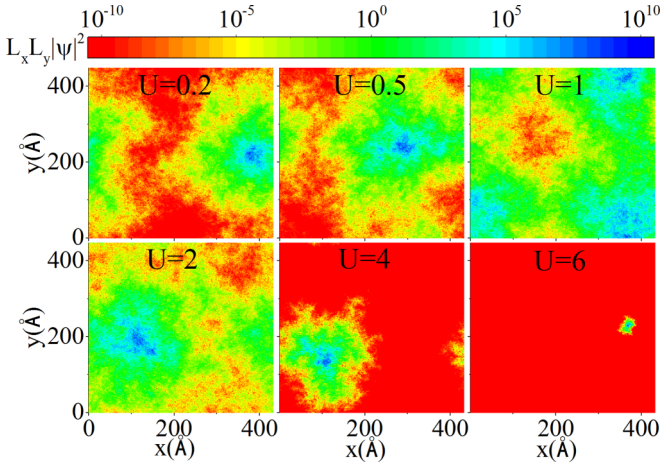

FIG. 3. Interaction dependence of the charge density (arbitrary units) at the Fermi energy for $W = 6$ for the honeycomb lattice of graphene. The size of the system is indicated in Angstroms. The eigenstates are localized for small interaction strengths $U = 0.2, 0.5$ and very large $U = 4, 6$. In the intermediate strengths, despite apparent percolation of the charge density which suggests a metallic state, it is not enough to specify the nature of the intermediate regime.

C. Characterization of intermediate regime with transfer matrix

Let us return to the metallic-looking phase for $U \sim 1$–2. As pointed out, even the sizes indicated in Fig. 3 are not enough to judge whether the system is Anderson localized, or the wave functions at the Fermi level are conducting. To make a conclusive judgment about the nature of this intermediate regime, we need to investigate much larger sizes where the methods such as exact diagonalization do not work. To overcome this problem, we employ the transfer matrix method (explained in Appendix C) and combine it with the local self-energy of the strong-coupling perturbation theory.

In Fig. 4, we plot the localization length (λ) normalized to the ribbon width (M) at zero energy for lattice with length $L = 10^5$ at disorder strength $W = 6$. The essential advantage of using the strong-coupling approach is that we can study very large lattices. This is in bold contrast to numerical methods such as exact diagonalization which suffer from finite-size limitations. In Fig. 4(a) the normalized localization length is plotted as a function of Hubbard U for various values of the ribbon width M indicated in the legend. In Fig. 4(b), we illustrate the normalized localization length as a function of M for various values of U. As can be seen in Fig. 4(a), the normalized localization length reaches a maximum value for all the ribbon widths. This maximum takes place for $U \approx 1.39$ which indeed corresponds to the percolation-looking structure in Fig. 3. This behavior is in agreement with previous works where the authors have computed the disorder-averaged inverse participation ratio [27,40]. As far as Fig. 3 is concerned, it is tempting to interpret the intermediate regime $U \sim 1$–2 as a metallic state. However as can be seen in Fig. 4(b), the scaling behavior of the normalized localization length with the ribbon width M is identical for all U values shown in the figure. So, in terms of the localization length, the intermediate regime, i.e., $U \sim 1$–2, is not different from the other values of

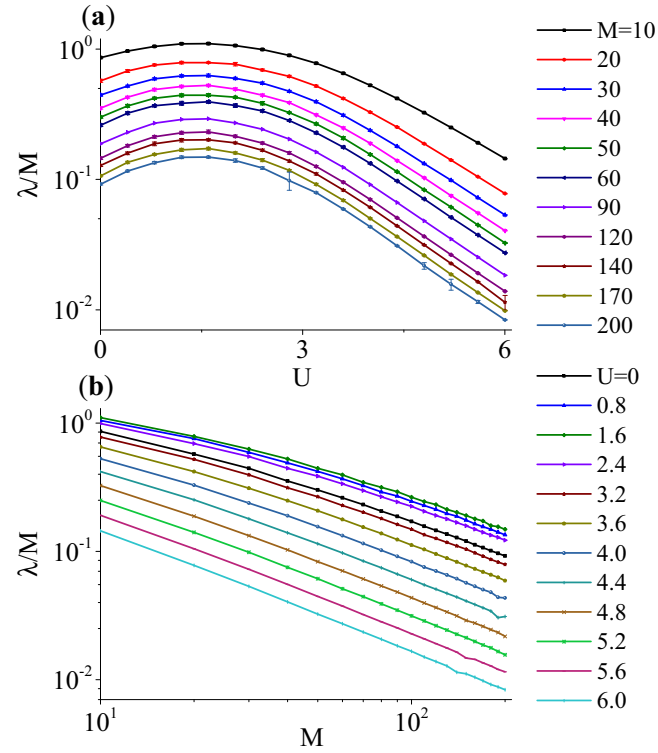

FIG. 4. The localization length normalized to the width, in ribbon geometry, at the Fermi level as a function of (a) interaction strength U for various ribbon widths M indicated in the legend, and (b) the ribbon width M for various Hubbard U values. In both cases, the disorder strength is fixed at $W = 6$ and lattice length $L = 10^5$. The apparent percolation structure in Fig. 3 for $U \sim 1$–2 corresponds to a maximum of localization length in panel (a) above. However, the finite-size scaling in (b) indicates that scaling behavior of the normalized localization length in the intermediate values $U \sim 1$–2 is no different from the other values.

U as long as there is no Mott gap in the spectrum. They all correspond to the Anderson localized states.

As can be seen in Fig. 4(b), for almost all values of U (up to $U \approx W$), the log-scale plots of λ/M versus M appear to be parallel lines. This feature suggests a relation of the form

$$\frac{\lambda}{M} = M^{-1/\nu} e^{f(U)}. \tag{11}$$

In Fig. 5 we have performed this scaling where the solid line is the form of the function $f(U)$. There is slight blurring in the data, which can be attributed to very weak dependence of the scaling exponent ν on U. In this language, the intermediate region, i.e., $U \sim 1$–2, corresponds to a maximum of the coefficient $\exp(f(U))$ and does not change the localized nature of the Fermi level wave functions which is given by *almost U independent* value $\nu = 1.38 \pm 0.16$. The scaling function f formalizes the idea of the screening of disorder by Hubbard interaction U. Increasing the interaction strengths from $U = 0$, the localization length increases until it reaches a maximum at $U_0 \approx 1.39$. This tendency of the Fermi level states to become less localized can be interpreted as the screening of the disorder by interactions. Beyond U_0, the screening is

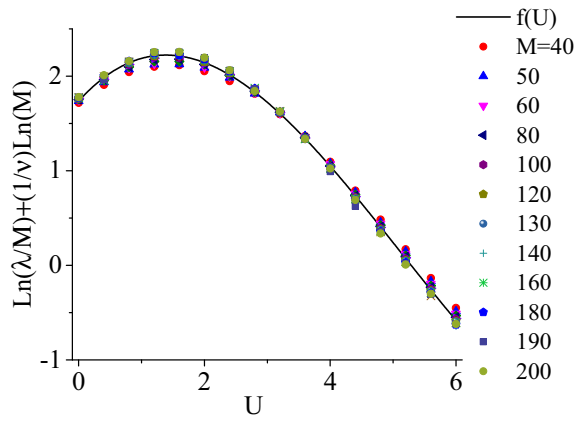

FIG. 5. Scaling analysis corresponding to Eq. (11) on data of Fig. 4. The exponent $\nu = 1.38 \pm 0.16$ has a very weak dependence on U. This figure is produced for disorder strength $W = 6$.

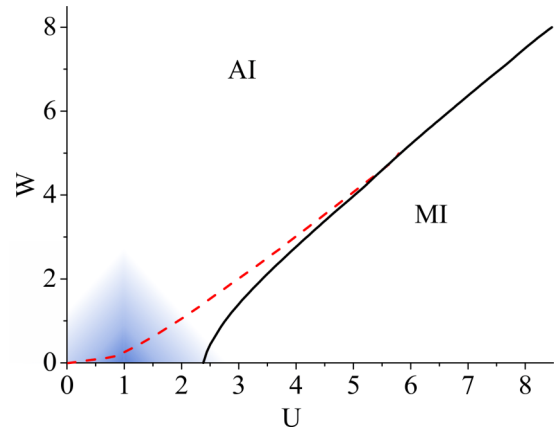

FIG. 6. Phase diagram in the UW plane for the Anderson-Hubbard model on the honeycomb lattice at half-filling and zero temperature. AI and MI refer to Anderson and Mott insulator, respectively. The dashed line indicates where the spectral gap appears, while the solid line represents where the extrapolated gap from the Mott side closes.

saturated and, consequently, the localization length decreases again, which is reflected as the decreasing behavior of $f(U)$.

When does the Anderson localized phase end? According to Fig. 5, after the localization length reaches a maximum, that corresponds to saturated screening, it starts to fall off. Therefore, by further increasing of the Hubbard interaction U, the wave functions at the Fermi level will become more and more localized. However, the localization on the right side of this maximum is driven by the Mottness tendency and is controlled by the Hubbard U. Ultimately, when the localization length λ reaches the lattice scale, i.e., $\lambda \sim 1$, the localized wave function will recognize its ultraviolet (UV) lattice, and therefore the low-energy states at the Fermi level now can sense the UV lattice. Indeed, the holographic Mott insulator corresponds precisely to an appearance of the UV lattice scale in the infrared (i.e., at Fermi level) [45]. Beyond this point where the system becomes Mott insulator, there will be no states at zero energy, i.e., all soft fermionic charge modes are gapped out.

The strong-coupling perturbation method used to address the Hubbard part of the Hamiltonian is based on the large-U limit. At the leading order of t/U considered in this paper, the method is expected to work better at larger U. Indeed, at small U, any values of U produce a spectral gap which has been denoted by the dashed line in Fig. 6. This fault is a known pathology of this method. The solution is to find out the gap for large values of U, and then to extrapolate the gap trend [10,46]. The extrapolation gives a better estimate of the critical U needed for Mott transition. This idea can also be applied to the disordered problem. For a given W, we start from large interaction strengths U and use the extrapolation to find the gap for smaller values of U. The results give the solid line in Fig. 6. For large enough U where the dashed and solid boundaries in Fig. 6 agree, the transfer matrix computation of the localization length works very well, and the onset of Mott gap opening is where the localization length becomes of the order of the lattice scale. By reducing W, the transfer matrix method starts to sense the scale lattice when it hits the dashed line. This limit, however, does not coincide with the onset of true Mott gap (solid line). The reason is that the strong-coupling expansion being an expansion in powers of t/U is reliable for large enough U, and consequently the extrapolation of the gap from the large-U (Mott) side is more reliable. Therefore, for the region of small U and small W indicated by shaded area, around $U/t \sim 1$ which can not be reached by perturbation from either side, the present method can not determine whether there is any conducting phase between the Anderson and Mott insulator or not. Exact QMC calculation by Ma and co-workers suggests a novel insulating phase rather than a metallic phase for a system with linearly vanishing density of states near the Fermi level [47]. However, for large enough U and W, the present method supported by finite-size scaling completely rules out the possibility of a conducting phase between Anderson and Mott insulators. Therefore, the conclusion is that for large enough Hubbard U, there is a critical W beyond which the system directly transforms from Mott localized phase to Anderson localized phase. The equivalent picture if one walks along a fixed W line is that for a fixed strong disorder W, beyond a critical U there will be a direct transition from Anderson insulating state to Mott insulating state. The phase diagram of the Coulomb interaction U versus the strength of disorder W at zero temperature and half-filling in Fig. 6 shows that two insulating phases are separated roughly at $U \approx W$ which is consistent with results of a self-consistent study [27] and DMFT calculation [40] in two dimensions. In the three dimensions, a similar picture is obtained by the QMC method [48]. An infinite-dimensional version of DMFT gives a similar picture [43].

IV. SUMMARY AND DISCUSSION

We have studied the competition of disorder and electron-electron interaction on the honeycomb lattice. To this end, we have investigated the Anderson-Hubbard model with the diagonal disorder at half-filling. The analytic and local structure of the strong-coupling perturbation method which we have used to treat the Hubbard part of the Hamiltonian allows us to address very large lattice sizes. To investigate the influence of the interaction on disordered electrons on the

honeycomb lattice, we calculate the disorder-averaged DOS using KPM. By employing the transfer matrix method in the ribbon geometry, we are able to perform a reliable finite-size scaling analysis which along the length of the ribbon (being based on transfer matrix) is essentially free from finite-size errors. For strong enough U and W, our finite-size scaling rules out the possibility of any metallic state between the Mott and Anderson insulating states. We, therefore, find a direct transition between Anderson and Mott states. However, the possibility of a novel insulating state [47] can not be ruled out by our analysis based on the localization length. The results indicate that the disorder shifts the Mott transition to larger values of the Hubbard U. Besides, the separation line of the Mott insulator and Anderson insulator is calculated from the criterion of vanishing of the single-particle gap which is extracted from DOS. Two phases are separated at $U \approx W$ for large interaction strengths. Despite limiting ourselves to the lowest-order perturbation theory, which is already enough to get the Mott transition in the clean limit, our results compare well with other numerical methods [27,40,41] in terms of the behavior of localization length in the presence of the ineraction. We found an interaction-induced enhancement of the localization length for weak and intermediate interaction strengths which is due to disorder screening. Although the localization length is enhanced in this way, it still remains finite. For large interaction due to the suppression of hopping, the localization length decreases as the Mott localization starts to take over. It is curious to note that at the onset of Mott insulation, the localization length becomes comparable to the lattice scale. This is similar to the holographic description of the Mott phase which is identified as a phase where at the low-energy (IR) limit (corresponding to states at the Fermi level), the system starts to recognize its UV lattice scale [45].

Before ending the paper, let us critically compare our finding of the absence of metallic phase between Mott and Anderson insulating states presented in Fig. 6 with other published works which used the box distribution for disorder. In Ref. [26] by self-consistent Hartree-Fock calculations for a 50×50 lattice in two dimensions, a metallic phase sandwiched between Anderson insulator and Mott insulating state was obtained. In this reference, the physics of strong correlation (Mott transition) could not be addressed, as they used a mean field factorization of the Hubbard interaction, and hence they found a metallic state. In Ref. [41] the considerable influence of the Hubbard repulsion U on delocalization was reported based on the results of the QMC method for lattices consisting of up to 6×8 sites. Because of numerical restrictions, the Anderson insulator to metal transition in thermodynamic limit was not concluded. This is because the maximum lattice size of 6×8 was not conclusive to establish a metallic state in the thermodynamic limit. A possible metallic phase in-between Anderson insulator and Mott insulator has been claimed by other studies based on QMC studies [24,25] in two dimensions as well as the results obtained from DMFT in infinite dimension [43] at half-filling. Additionally, a study based on the dual-fermion approach in three dimensions [44] claims the existence of the metallic phase in weak interaction strengths. All the above works have been done on lattices with a small number of sites. Thus, in these studies, a very severe finite-size effect is inevitable. The finite-size effects become even more severe for honeycomb lattice where (due to Dirac nature of electrons) the localization length at small values of disorder is very large. On the other hand, authors of a statistical DMFT study [40] on the two-dimensional lattice with up to 1000 sites did not find insulator-metal transition at strong disorder strengths which coincide with what we presented in Fig. 6. Moreover, the authors of Ref. [27] using a self-consistent calculation showed that existence of the metal phase is impossible.

ACKNOWLEDGMENT

S.A.J. was supported by Iran Science Elites Federation (ISEF).

APPENDIX A: ONE-POINT CONNECTED CORRELATION FUNCTION

This Appendix gives the one-point correlation function of the atomic limit of the Anderson-Hubbard model. We consider the unperturbed Hamiltonian H_0 of Eq. (1) as $H_0 = \sum_i h_i$ where h_i is expressed as

$$h_i = U n_{i\uparrow} n_{i\downarrow} - \mu \sum_\sigma n_{i\sigma} + \sum_\sigma \epsilon_i \, n_{i\sigma}. \tag{A1}$$

The one-point connected correlation function is defined as

$$\mathcal{G}_{i\sigma}(\tau, 0) = -\langle T_\tau \, c_{i\sigma}(\tau) \, c^\dagger_{i\sigma}(0)\rangle, \tag{A2}$$

where T_τ represents the time-ordering operator and the average is calculated with respect to local Hamiltonian h_i. Note that in the absence of magnetic field in the Hamiltonian (A1), we can not distinguish between the one-point connected correlation functions of the two spin projections $\sigma = \uparrow, \downarrow$. Let us rewrite the one-point connected correlation function as follows:

$$\mathcal{G}_{i\sigma}(\tau, 0) = -\frac{1}{Z} \, \mathrm{Tr} \, (e^{-\beta h_i} \, c_{i\sigma}(\tau) \, c^\dagger_{i\sigma}),$$

where the partition function Z is given by

$$Z = 1 + 2e^{\beta(\mu - \epsilon_i)} + e^{\beta(2\mu - 2\epsilon_i - U)}. \tag{A3}$$

The one-point connected correlation function can be computed by inserting the identity operator

$$\mathcal{G}_{i\sigma}(\tau, 0) = -\frac{1}{Z} \sum_{nn'} \langle n | e^{-\beta h_i} e^{\tau h_i} c_{i\sigma} e^{-\tau h_i} | n' \rangle \langle n' | c^\dagger_{i\sigma} \, | n \rangle,$$

where the $|n\rangle$ and $|n'\rangle$ states denote the four possible states of the Hilbert space at each site $|0\rangle$, $|\sigma\rangle$, $|\bar{\sigma}\rangle$, and $|\uparrow\downarrow\rangle$ which correspond to the empty, single occupied states with spin projection σ and its opposite projection $\bar{\sigma}$, and doubly occupied state, respectively. The nonzero terms are given as follows:

$$\mathcal{G}_{i\sigma}(\tau, 0) = -\frac{1}{Z} \, \langle 0 | e^{-\beta h_i} \, e^{\tau h_i} \, c_{i\sigma} \, e^{-\tau h_i} | \sigma \rangle \langle \sigma | c^\dagger_{i\sigma} | 0 \rangle - \frac{1}{Z} \, \langle \bar{\sigma} | e^{-\beta h_i} \, e^{\tau h_i} \, c_{i\sigma} \, e^{-\tau h_i} | \uparrow \downarrow \rangle \langle \uparrow \downarrow | c^\dagger_{i\sigma} | \bar{\sigma} \rangle.$$

So, we obtain

$$\mathcal{G}_{i\sigma}(\tau, 0) = -\frac{1}{Z} \left(e^{\tau(\mu - \epsilon_i)} + e^{\beta(\mu - \epsilon_i)} e^{\tau(\mu - \epsilon_i - U)} \right). \tag{A4}$$

Fourier transforming to Matsubara frequencies, we have

$$\mathcal{G}_{i\sigma}(i\omega) = \int_0^\beta d\tau\, e^{i\omega\tau}\, \mathcal{G}_{i\sigma}(\tau, 0) = \frac{1}{Z}\,\frac{1+e^{\beta(\mu-\epsilon_i)}}{i\omega+\mu-\epsilon_i} + \frac{1}{Z}\,\frac{e^{\beta(2\mu-2\epsilon_i-U)}+e^{\beta(\mu-\epsilon_i)}}{i\omega+\mu-\epsilon_i-U}. \tag{A5}$$

By introducing the mean occupation $\langle n_i\rangle$ for each spin and lattice site i as

$$\langle n_i\rangle = \frac{e^{\beta(\mu-\epsilon_i)}+e^{\beta(2\mu-2\epsilon_i-U)}}{Z}, \tag{A6}$$

the one-point connected correlation function at arbitrary temperature $1/\beta$ becomes

$$\mathcal{G}_{i\sigma}(i\omega) = \frac{1-\langle n_i\rangle}{i\omega+\mu-\epsilon_i} + \frac{\langle n_i\rangle}{i\omega+\mu-\epsilon_i-U}. \tag{A7}$$

At zero-temperature limit or equivalently $\beta\to\infty$, the one-point connected correlation function is simplified to

$$\mathcal{G}_{i\sigma}(i\omega) = \frac{\Theta(\epsilon_i-\mu)}{i\omega+\mu-\epsilon_i} + \frac{1}{2}\frac{\Theta(\epsilon_i-\mu+U)\,\Theta(\mu-\epsilon_i)}{i\omega+\mu-\epsilon_i} + \frac{\Theta(\mu-\epsilon_i-U)}{i\omega+\mu-\epsilon_i-U} + \frac{1}{2}\frac{\Theta(\epsilon_i-\mu+U)\Theta(\mu-\epsilon_i)}{i\omega+\mu-\epsilon_i-U}. \tag{A8}$$

APPENDIX B: KERNEL POLYNOMIAL METHOD

Generally speaking, KPM is a numerical approach to calculate the spectral functions based on their expanding in Chebyshev polynomials [36,37]. Then, the expansion coefficients computed stochastically. So, we can expand the DOS as follows:

$$\hat{\rho}(\epsilon) = \frac{1}{\pi\sqrt{1-\epsilon^2}}\left(\mu_0\, g_0 + 2\sum_{l=1}^{N_c}\mu_l\, g_l\, T_l(\epsilon)\right), \tag{B1}$$

where ϵ is rescaled energy in such a way that fits in the range $[-1,1]$, $T_l(\epsilon)=\cos(l\arccos(\epsilon))$ is lth Chebyshev polynomial, g_l's are the Jackson kernel coefficients which minimize the Gibbs oscillations, and μ_l are Chebyshev moments. The sum is taken up to a cutoff number N_c. It is important to note that in this method the Hamiltonian $H(E)$ with energy spectrum between $[E_{\min}, E_{\max}]$ is rescaled to $\hat{H}(\epsilon)$ where $\hat{H}=(H-b)/a$, $\epsilon=(E-b)/a$, $b=(E_{\max}+E_{\min})/2$, and $a=(E_{\max}-E_{\min})/2$. Also, the moments are given by

$$\mu_l = \frac{1}{M}\sum_{r=1}^{M}\langle\phi_r|T_l(\hat{H})|\phi_r\rangle, \tag{B2}$$

where ϕ_r are random single-particle states and M is the number of random states used in numerical calculations. Furthermore, one can obtain the effect of $T_l(\hat{H})$ on a given ket using the recurrence relation of Chebyshev polynomials, namely, $T_l(\hat{H})=2\hat{H}T_{l-1}(\hat{H})-T_{l-2}(\hat{H})$ with initial conditions $T_1(\hat{H})=\hat{H}$ and $T_0(\hat{H})=1$.

To calculate the DOS for the Green's function in Eq. (7), we use the following trick:

$$\rho'(\omega) = -\frac{1}{\pi}\lim_{\eta\to0}\mathrm{Im}\left[\mathrm{Tr}\frac{1}{E+i\eta+\Gamma^{-1}(i\omega)-V}\Big|_{E=0}\right]. \tag{B3}$$

Thus, Eq. (B1) can be rewritten as

$$\hat{\rho}'(\omega') = \frac{1}{\pi\sqrt{1-\epsilon^2}}\left(\mu_0\, g_0 + 2\sum_{l=1}^{N_c}\mu_l(\omega')\, g_l\, T_l(\epsilon)\right)\Big|_{\epsilon=0}, \tag{B4}$$

where $\mu_l(\omega')$ are the generalized KPM coefficients in which $H=\Gamma^{-1}(\omega)-V$. Also, ω' and $\hat{H}$ denote the rescaled ω and H, respectively. To calculate $\mu_l(\omega')$, we need to compute μ_l for every ω' which is a computationally expensive part of the calculations. So, we have used MPICH package to parallelize our program. Additionally, due to divergences of $\Gamma^{-1}(\omega)$ for some values of disorder and to obtain a large bandwidth, we set $N_c=15\,000$, $M=5$, and average it on 100 configurations to obtain well-converged values of DOS $\rho'(\omega')$ at $E=0$.

APPENDIX C: TRANSFER MATRIX METHOD

In this Appendix, we briefly explain the transfer matrix method we have used [49] to calculate the localization length [38,39]. The localization length λ of the quasi-one-dimensional system is defined as the characteristic length that specifies the exponential decay of wave function with the system length L [50]:

$$\psi(L)\ \propto\ \exp(-L/\lambda). \tag{C1}$$

In the transfer matrix method, the quasi-one-dimensional Schrödinger equation $\hat{H}\vec{\Psi}_i=E\vec{\Psi}_i$ is written as

$$\hat{V}^*_{i,i-1}\vec{\Psi}_{i-1}+\hat{H}_{i,i}\vec{\Psi}_i+\hat{V}_{i,i+1}\vec{\Psi}_{i+1}=E\vec{\Psi}_i. \tag{C2}$$

So, the wave function $\vec{\Psi}_i$ of the ith slice along the transfer direction is iteratively calculated using the following transfer matrix equation:

$$\begin{pmatrix}\vec{\Psi}_{i+1}\\ \vec{\Psi}_i\end{pmatrix} = \hat{T}_{i+1,i}\begin{pmatrix}\vec{\Psi}_i\\ \vec{\Psi}_{i-1}\end{pmatrix}, \tag{C3}$$

where

$$\hat{T}_{i+1,i} = \begin{pmatrix}\hat{V}^{-1}_{i,i+1}(E\mathbb{1}-\hat{H}_{i,i}) & -\hat{V}^{-1}_{i,i+1}\,\hat{V}^*_{i,i-1}\\ \mathbb{1} & \mathbb{0}\end{pmatrix}. \tag{C4}$$

Here, all the vector elements are $M\times M$ matrices and T is $2M\times 2M$ matrix where M denotes to the width of the system. Since the transport is stronger along the zigzag edge, in this work, we assume the transfer direction along this edge with periodic boundary condition as depicted in Fig. 7.

According to Oseledec's theorem [51], in the thermodynamic limit, the eigenvalues of

$$\hat{\Gamma} = \lim_{N\to\infty}\left[\prod_{i=N}^{1}\hat{T}^\dagger_{i+1,i}\prod_{i=1}^{N}\hat{T}_{i+1,i}\right]^{1/2N} \tag{C5}$$

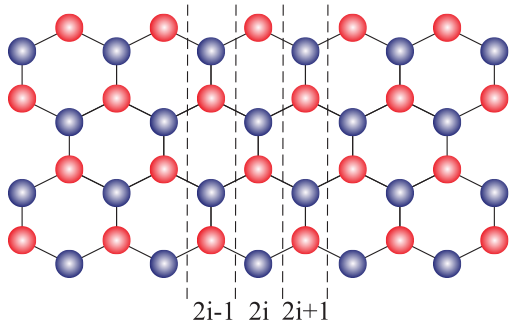

FIG. 7. The honeycomb lattice used for transfer matrix method with transfer direction along zigzag edge and width $M = 4$ and length $L = 11$.

converge to fixed values $e^{\pm\gamma_m}$ where γ_m with $m = 1, \ldots, M$ are Lyapunov exponents. The localization length can be defined as the largest decaying length related to the minimum Lyapunov exponent

$$\lambda = \frac{1}{\gamma_{\min}}. \tag{C6}$$

Practically, to avoid numerical overflow, which came from multiplying the transfer matrices in Eq. (C5), the Gram-Schmidt method is employed to orthonormalize the vectors. Let us note that we perform the Gram-Schmidt orthonormalization after each multiplication due to severe fluctuations of the localization length on the honeycomb lattice. Additionally, in our calculation, N is chosen in such a way that localization length converges.

[1] N. F. Mott, Proc. Phys. Soc. London, Sect. A **62**, 416 (1949).
[2] P. W. Anderson, Phys. Rev. **109**, 1492 (1958).
[3] S. Sorella, Y. Otsuka, and S. Yunoki, Sci. Rep. **2**, 992 (2012).
[4] Y. Otsuka, S. Yunoki, and S. Sorella, Phys. Rev. X **6**, 011029 (2016).
[5] I. F. Herbut and M. Oshikawa, Phys. Rev. Lett. **97**, 080403 (2006).
[6] S. Raghu, X.-L. Qi, C. Honerkamp, and S.-C. Zhang, Phys. Rev. Lett. **100**, 156401 (2008).
[7] R.-Q. He and Z.-Y. Lu, Phys. Rev. B **86**, 045105 (2012).
[8] W. Wu, Y.-H. Chen, H.-S. Tao, N.-H. Tong, and W.-M. Liu, Phys. Rev. B **82**, 245102 (2010).
[9] A. Liebsch, Phys. Rev. B **83**, 035113 (2011).
[10] E. Adibi and S. A. Jafari, Phys. Rev. B **93**, 075122 (2016).
[11] Y.-Y. Zhang, J. Hu, B. A. Bernevig, X. R. Wang, X. C. Xie, and W. M. Liu, Phys. Rev. Lett. **102**, 106401 (2009).
[12] E. R. Mucciolo and C. H. Lewenkopf, J. Phys.: Condens. Matter **22**, 273201 (2010).
[13] I. L. Aleiner and K. B. Efetov, Phys. Rev. Lett. **97**, 236801 (2006).
[14] A. Altland, Phys. Rev. Lett. **97**, 236802 (2006).
[15] S.-J. Xiong and Y. Xiong, Phys. Rev. B **76**, 214204 (2007).
[16] G. Schubert, J. Schleede, K. Byczuk, H. Fehske, and D. Vollhardt, Phys. Rev. B **81**, 155106 (2010).
[17] E. Abrahams, P. W. Anderson, D. C. Licciardello, and T. V. Ramakrishnan, Phys. Rev. Lett. **42**, 673 (1979).
[18] M. Schreiber and M. Ottomeier, J. Phys.: Condens. Matter **4**, 1959 (1992).
[19] Z. Fan, A. Uppstu, and A. Harju, Phys. Rev. B **89**, 245422 (2014).
[20] K. L. Lee, B. Grémaud, C. Miniatura, and D. Delande, Phys. Rev. B **87**, 144202 (2013).
[21] M. Amini, S. A. Jafari, and F. Shahbazi, Europhys. Lett. **87**, 37002 (2009).
[22] Y. Song, H. Song, and S. Feng, J. Phys.: Condens. Matter **23**, 205501 (2011).
[23] P. J. H. Denteneer, R. T. Scalettar, and N. Trivedi, Phys. Rev. Lett. **83**, 4610 (1999).
[24] P. J. H. Denteneer and R. T. Scalettar, Phys. Rev. Lett. **90**, 246401 (2003).
[25] P. B. Chakraborty, P. J. H. Denteneer, and R. T. Scalettar, Phys. Rev. B **75**, 125117 (2007).
[26] D. Heidarian and N. Trivedi, Phys. Rev. Lett. **93**, 126401 (2004).
[27] P. Henseler, J. Kroha, and B. Shapiro, Phys. Rev. B **78**, 235116 (2008).
[28] Z. Meng, T. Lang, S. Wessel, F. Assaad, and A. Muramatsu, Nature (London) **464**, 847 (2010).
[29] A. Moreo, D. J. Scalapino, R. L. Sugar, S. R. White, and N. E. Bickers, Phys. Rev. B **41**, 2313 (1990).
[30] C. Noce and M. Cuoco, Phys. Rev. B **54**, 13047 (1996).
[31] H. Park, K. Haule, and G. Kotliar, Phys. Rev. Lett. **101**, 186403 (2008).
[32] K. Seki and Y. Ohta, arXiv:1209.2101.
[33] M. Balzer, B. Kyung, D. Sénéchal, A.-M. Tremblay, and M. Potthoff, Europhys. Lett. **85**, 17002 (2009).
[34] S. Pairault, D. Sénéchal, and A.-M. S. Tremblay, Phys. Rev. Lett. **80**, 5389 (1998).
[35] S. Pairault, D. Sénéchal, and A.-M. Tremblay, Eur. Phys. J. B **16**, 85 (2000).
[36] A. Weiße, G. Wellein, A. Alvermann, and H. Fehske, Rev. Mod. Phys. **78**, 275 (2006).
[37] A. Habibi and S. A. Jafari, J. Phys.: Condens. Matter **25**, 375501 (2013).
[38] A. MacKinnon and B. Kramer, Phys. Rev. Lett. **47**, 1546 (1981).
[39] A. MacKinnon and B. Kramer, Z. Phys. B **53**, 1 (1983).
[40] Y. Song, R. Wortis, and W. A. Atkinson, Phys. Rev. B **77**, 054202 (2008).
[41] B. Srinivasan, G. Benenti, and D. L. Shepelyansky, Phys. Rev. B **67**, 205112 (2003).
[42] S. Reich, J. Maultzsch, C. Thomsen, and P. Ordejon, Phys. Rev. B **66**, 035412 (2002).
[43] K. Byczuk, W. Hofstetter, and D. Vollhardt, Phys. Rev. Lett. **94**, 056404 (2005).

[44] P. Haase, S.-X. Yang, T. Pruschke, J. Moreno, and M. Jarrell, Phys. Rev. B **95**, 045130 (2017).
[45] A. Donos and S. A. Hartnoll, arXiv:1212.2998.
[46] P. Sahebsara and D. Sénéchal, Phys. Rev. Lett. **100**, 136402 (2008).
[47] T. Ma, L. Zhang, C.-C. Chang, H.-H. Hung, and R. T. Scalettar, Phys. Rev. Lett. **120**, 116601 (2018).
[48] Y. Otsuka and Y. Hatsugai, J. Phys.: Condens. Matter **12**, 9317 (2000).
[49] A. Habibi, S. A. Jafari, and S. Rouhani, Phys. Rev. B **98**, 035142 (2018).
[50] M. Janssen, Phys. Rep. **295**, 1 (1998).
[51] V. I. Oseledets, Tr. Mosk. Mat. Obs. **19**, 179 (1968).